ISBN: 978-3-95450-192-2 doi:10.18429/JACoW-IBIC2017-TH1AB2

BEAM CONTAINMENT AND MACHINE PROTECTION FOR LCLS-2*

Alan S. Fisher†, Christine Clarke, Clive Field, Josef Frisch, Ryan Herbst,
Ruslan Kadyrov, Bobby McKee, Feng Tao, James Welch,
SLAC National Accelerator Laboratory, Menlo Park, California 94027, USA

Abstract

The first km of the 3-km SLAC linac is being replaced by LCLS-2, a superconducting linac with continuous RF and a maximum beam rate of 1 MHz. The beam will have an energy of 4 GeV and a maximum power of 250 kW, with an upgrade to 8 GeV and 1.2 MW in planning. The beam will be transported through the accelerator tunnel, passing over the future 1-km FACET-2 and the existing 1-km LCLS linacs, both using normal-conducting copper cavities at repetition rates of up to 30 and 120 Hz respectively. The LCLS and LCLS-2 beams will continue together through the Beam Transport Hall to two new undulators, for hard and soft x rays. Kickers will direct individual pulses to either undulator or to a dump. The high power in the beam and potentially in field emission necessitates integrating losses over 500 ms but responding within 0.1 ms. A capacitor for integration and a comparator for the threshold give a simple and robust approach over a wide dynamic range. We plan both long loss monitors covering regions of typically 100 m and point monitors. In regions with two or more beamlines, the system will attempt to determine the line that caused a loss, so that only one is shut off.

INTRODUCTION

LCLS, LCLS-2, and FACET-2

The LCLS x-ray free-electron laser (FEL) at SLAC National Accelerator Laboratory began operation in 2009 [1] using the third kilometre of SLAC's 3-km linear accelerator. It retains the original 2856-MHz copper linac, but with a 1.6-cell copper radio-frequency (RF) photocathode gun at 2856 MHz. Both are pulsed at 120 Hz.

LCLS-2 [2] will replace the first km of the copper linac, removed one year ago, with a superconducting linac using continuous RF at 1300 MHz. Laser pulses at rates of up to 1 MHz will emit electrons from a normal-conducting photocathode gun with 186-MHz (1300/7) continuous RF. Operation will begin at an electron energy of 4 GeV and a maximum beam power of 250 kW. Upgrades will raise the beam energy to 8 GeV and the power to 1.2 MW, as shown in Table 1. This high beam power demands fast but accurate response to beam losses.

The middle km of the linac tunnel will be occupied by FACET-2, a user facility mainly for advanced acceleration studies [3]. The LCLS-2 beam will bypass both FACET-2 and LCLS in a transport line suspended from the tunnel ceiling and only 125 cm from the two linac beams, which may make it difficult at times to determine unambiguously the source of a loss signal.

* SLAC is supported by the U.S. Department of Energy under contract DE-AC02-76SF00515.
† afisher@slac.stanford.edu

Table 1: Parameters for LCLS and LCLS-2

Parameter	LCLS	LCLS-2
Electron energy	15 GeV	4 (later 8) GeV
Bunch charge	20 to 250 pC	20 to 300 pC
Beam power	450 W	**0.25 (later 1.2) MW**
Gun frequency	2856 MHz	185.7 MHz
Linac frequency	2856 MHz	1300 MHz
RF pulse rate	120 Hz	Continuous
e^- bunch rate	120 Hz	92.9 (later 929) kHz
Photon energy	0.2 to 12 keV	1 to 15 (later 25) keV

Safety Systems for Beam Loss

SLAC uses a three-tier protection system. The highest, the Personnel Protection System (PPS), prevents unsafe machine access. The Beam Containment System (BCS) stops the accelerator if a loss of beam current or radiation from beam loss indicates possible harm to people or to safety devices like protection collimators. It must be robust and simple, with no knowledge of bunch timing and no software. As safety systems, both have rigorous configuration control. The Machine Protection System (MPS) is more flexible. When triggered—for example, by high losses, the insertion of an obstacle such as a valve, an excessive temperature—MPS can insert a beam stop, lower the beam rate, block the photocathode laser, or halt the beam. Recovery from an MPS event is faster than from a BCS trip, and so its thresholds are set lower.

LCLS-2 beam-loss detectors will serve three purposes: BCS, MPS, and beam diagnostics. Losses below the trip thresholds will provide diagnostic information to operators for tuning the machine and locating high-loss points to avoid or recover from a rate limit or trip.

Trip specifications vary with the tunnel depth and other shielding and are given in joules of beam loss within an integration time of 500 ms. BCS thresholds range from 500 to 17.5 J. MPS thresholds are generally set 10 times lower. This loss can arrive in a fast burst of lost photocurrent or slowly over the full integration time. The repetition rate of the losses can be at any beam rate from 10 Hz to 1 MHz; a full loss of 1-Hz beam is permitted for tuning. Field emission (dark current) from the gun or linac may generate loss in every RF period (Table 1) and would appear as a DC signal in the loss detectors.

LCLS BEAM-LOSS MONITORS

BCS and MPS at SLAC have long used ionization chambers. A Protection Ion Chamber (PIC), an array of interleaved circular parallel plates, is placed at each expected loss point. A long ionization chamber (LION)

ISBN: 978-3-95450-192-2 doi:10.18429/JACoW-IBIC2017-TH1AB2

using a gas-dielectric Heliax coaxial cable (nominal 1⅝ inch) runs parallel to the beam to cover an extended region. The performance of these detectors for the high-power LCLS-2 beam is problematic due to the slow transit time of ions (>1 ms). An earlier study of loss detection for LCLS-2 [4] showed that ion accumulation can fully screen the electric field in a field-free "dead zone" growing from the positive electrode. That report presented initial tests of the alternative detectors discussed below.

LCLS-2 LONG BEAM-LOSS MONITORS

Optical Fibres

In place of LIONs, we have investigated Cherenkov emission in a radiation-hard optical fibre, FBP600660710 from the Polymicro division of Molex. This high-OH^- quartz fibre has a 600-µm-diameter core, a 660-µm cladding, and a 2-mm-diameter outer protective jacket of black polyurethane. Short fibres of this family were tested to 1.25 Grad for use at CERN in the CMS detector's end cap [5,6]. Using the study's parameterization of attenuation as a function of wavelength and dose, we computed the attenuation in a 100-m fibre at LCLS-2. The calculation made the conservative assumption that a 10-m length of this fibre is constantly irradiated without tripping; the other 90 m remains unexposed. A FLUKA simulation [7] of the radiation field converts lost beam power to dose rate. A constant 50-J loss in 500 ms, the linac's MPS limit, corresponds to 25 Mrad/yr at a distance of 50 cm.

Choice of Wavelength

Figure 1 plots attenuation in a 100-m fibre as a function of wavelength for doses up to 25 Mrad. For a reasonably uniform response, we set the criterion that a loss at the end of the fibre far from the light detector should be no more than 3 dB below a loss at the near end, after irradiation. The longer wavelengths are clearly preferable before exposure and far better after the maximum dose.

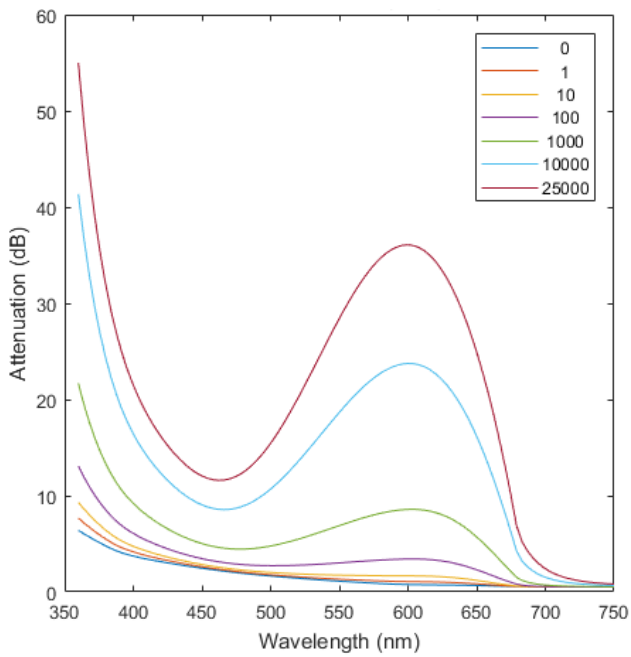

Figure 1: Calculated attenuation in a 100-m-long fibre vs. wavelength, for various radiation doses (krad) to 10 m.

Cherenkov emission is blue, since its intensity $dI/dxd\omega$ is proportional to ω. However, the signal at 700 nm can be adequate since detectors respond to the photon flux $dN/dxd\omega$, which is flat with frequency (although, in terms of wavelength, $dN/dxd\lambda \sim \lambda^{-2}$).

The photocathode work function in a red-sensitive photomultiplier (PMT) is low. This increases dark current, which should be limited to 1 nA for sensitivity to field emission from the gun and linac. Cooling from 20 to 0°C reduces dark current by a factor of 9 in a multialkali PMT [8]; above 10°C, the change is exponential, 0.67 dB/°C. We are testing Hamamatsu's H7422P-40, a PMT module with a GaAsP photocathode having a 30% quantum efficiency at 700 nm, and housed in an enclosure with a Peltier (thermoelectric) cooler holding a 0°C temperature.

A red long-wave-pass or band-pass filter makes the integrated signal largely independent of dose (although reducing the total signal). Figure 2 plots dose vs. the Cherenkov emission combined with the response of the fibre, PMT and filter, integrated over wavelength. An additional point indicates the loss for a fibre of negligible length without radiation, for comparison to 100 m. The long-pass filter doubles the band-pass signal and drops by less than the desired factor of 2 even at the highest dose.

Location of the Photomultiplier

Cherenkov light couples into fibre modes travelling in both directions. Each end of the fibre offers advantages as the PMT location. If electrons passing the start ($z = 0$) of a

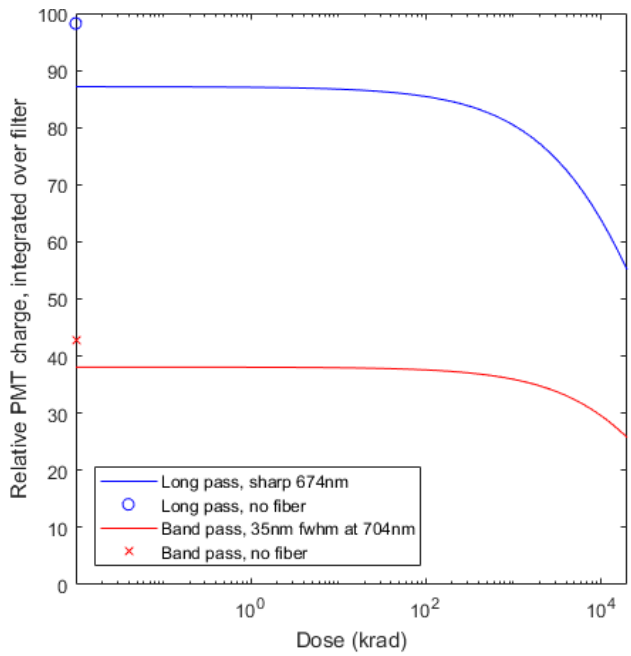

Figure 2: Cherenkov emission integrated over the PMT response and the band of a red filter for a 100-m fibre. Before 10 m of the fibre is irradiated over 10 m, the attenuation is about 10% compared to a fibre of negligible length, and is maintained until the dose exceeds 100 krad.

ISBN: 978-3-95450-192-2 doi:10.18429/JACoW-IBIC2017-TH1AB2

fibre of length L at $t = 0$ are lost at z, the upstream signal (at PMT1) reaches z = 0 at $t_u(z) = (1+n)z/c$, where the refractive index $n \approx 1.5$. The downstream signal (PMT2) arrives at L at $t_d(z) = (1-n)z/c+Ln/c$. Two losses a distance Δz apart produce PMT signals separated by $\Delta t_u = (1+n)\Delta z/c \approx 2.5\Delta z/c$ and $\Delta t_d = (1-n)\Delta z/c \approx -0.5\Delta z/c$. The signals arrive at PMT2 in reverse order and closer by a factor of 5. This compression could simply rescale the time axis, but z resolution can be degraded by cable dispersion, PMT rise time or digitizer bandwidth.

The counter argument to placing the PMT at the upstream end is that the beam-loss shower is stronger in the forward direction: more Cherenkov light should couple into a fibre mode travelling downstream. Determining this effect by computation requires precise models of both the shower and the capture of Cherenkov light. Instead, we measured the effect using a PMT at each end of a 155-m fibre. Blue-sensitive PMTs (Hamamatsu R7400U-06), also allowed us to compare the measured and calculation attenuation, since the loss is higher over this distance.

Corrector magnets steered the beam into the beampipe to generate losses at various distances from a beam stopper at the downstream end. Loss signals (Fig. 3) at the PMTs show changes in both arrival time and amplitude. Figure 4 plots the signal ratio PMT1/PMT2. As the loss shifts downstream, the attenuation grows at PMT1 and drops at PMT2, doubling the attenuation (30 dB/km vs. 5 dB/km at 700 nm). A calculation using only the wavelength dependence of Cherenkov light, fibre and PMT determines the slope of the blue line. Its offset, chosen to fit the measurements, gives a backward/forward signal ratio of 27%. This is a convincing reason to put the PMTs at the downstream end. The upstream end will have an LED for periodic fibre testing and calibration, both to verify that the system is working (a "heartbeat") and to monitor the slow decrease in transmission with radiation.

Transverse Pattern of the Loss Shower

The transverse directionality of the loss shower was also tested. The fibre discussed above runs directly on the beampipe; in a different region, a 100-m fibre was placed 125 cm away from the beam. For both, we found little difference in the loss signals when steering the beam to the left, right, up and down, demonstrating that full coverage does not need multiple fibres. However, we will install two fibres in most places, for redundancy.

Each fibre will be installed in a metal conduit attached to the tunnel wall or to beamline supports. Each end will go an additional 15 m to a rack above the tunnel. This layout protects the fibre from mechanical damage, avoids long cables, prevents radiation damage to the PMT and LED, and makes it possible to install a replacement fibre without tunnel access. Each interface chassis will have two PMTs and two LEDs to receive four fibres.

LCLS-2 POINT BEAM-LOSS MONITORS

Diamond Detectors

We plan to use Cividec diamond detectors [9] in place of PICs as point loss monitors. The B2 polycrystalline type will be suitable for most locations. An earlier test [4] comparing diamonds to PICs showed that the diamond signals are faster and much less noisy. Diamonds also offer a dynamic range of 10^6. The PIC's dynamic range is limited by ion accumulation [4] and by an internal voltage divider providing an offset on the signal output to verify that the −300-V bias is present. The offset would blind the detector to small but steady field-emission losses.

We are investigating two concepts to verify the functionality of the diamonds without this offset. Ultraviolet with $\lambda < 225$ nm produces electron-hole pairs in diamond. The Cividec detector case has an opening over one side of the 8×8×0.5-mm^3 diamond chip, intended for calibration with an α-particle emitter through a 1-mm-diameter region without metallization. This allows a xenon flashlamp with a quartz envelope to produce a UV heartbeat (like the LED and fibre), as demonstrated in a test with a large xenon lamp. We will test a smaller Hamamatsu xenon lamp coupled to a UV-transmitting fibre that can be placed directly over the 1-mm circle.

The alternative is a voltage divider to monitor the 500-V bias. A fault would result from disconnecting either the bias or a dual connector grouping the monitor with the output signal. Although not as comprehensive as the UV

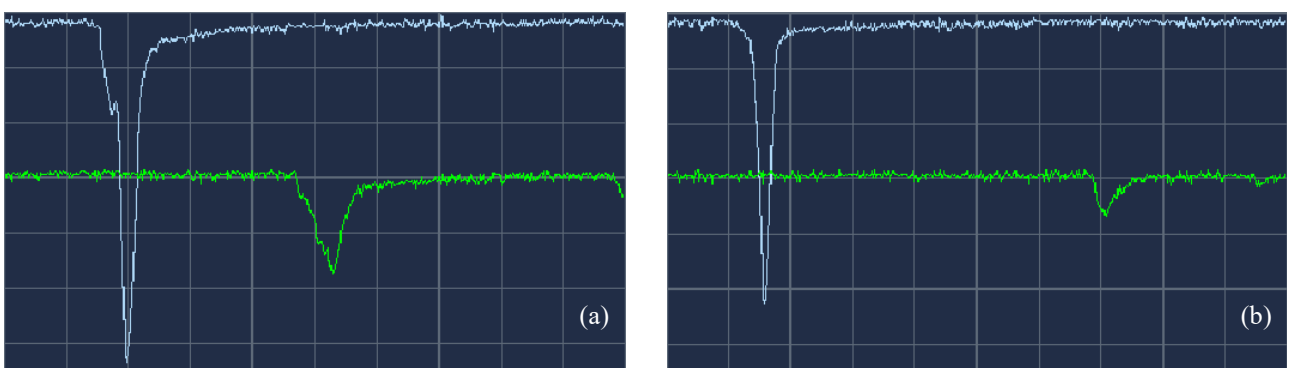

Figure 3: Signals from PMT1 (green trace, upstream end of fibre), and PMT2 (blue, downstream end); 200 ns/div and 1 V/div into 50 Ω. The loss points are (a) 82 m and (b) 39 m upstream of the beam stop at the downstream end. As the loss moves downstream, the peak decreases in amplitude and moves rightward for PMT1, but increases and moves leftward for PMT2. Relative to PMT1, the pulse widths and peak separations of PMT 2 are compressed by a factor of 5.

ISBN: 978-3-95450-192-2 doi:10.18429/JACoW-IBIC2017-TH1AB2

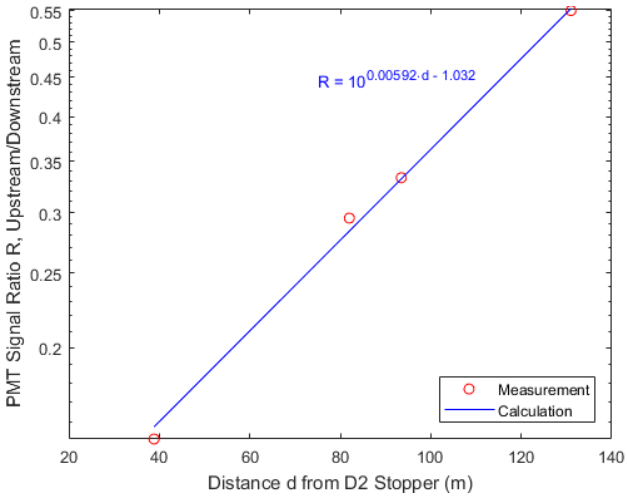

Figure 4: PMT1/PMT2 ratio. The calculated slope comes only from the properties of the Cherenkov light, fibre and PMT. The vertical offset, from a fit to the measurements, determined that the signal from the backward loss shower was 27% of the forward signal.

test, it is simpler and finds the most likely failure modes.

We rejected a third heartbeat idea—modulating the bias to produce a signal across the diamond's 10-pF capacitance—because the signal would be much too small at frequencies passed by the 500-ms filter discussed below.

SIGNAL PROCESSING

The charge in a single 1.3-GHz period of dark current can be as small as 10 aC; a single pulse of photocurrent may contain 250 pC. Digitizing pulse-by-pulse demands an unreasonable dynamic range. Instead, the PMT current will go to a filter, in which a capacitor integrates the low-frequency charge and a large parallel resistor provides the required 500-ms time constant. A comparator will trip the beam if the capacitor voltage exceeds the threshold. A buffer amplifier will pass this voltage to MPS. A second buffer will send high frequencies, needed for loss localization, to a waveform digitizer. Because the PMT will be in the chassis with the filter, cable capacitance will not alter the filter's behaviour.

The diamond must be in the tunnel at the loss point, and so requires a long cable. The diamond current will also be integrated on a capacitor. Cable capacitance is not a problem for low frequencies, and high frequencies are unnecessary without loss localization. The cable's leakage must be well below the large parallel load resistor giving the 500-ms time constant. This concern can be addressed with a low-leakage dielectric, such as solid polyethylene, or with triaxial cable in which the inner shield is driven to match the voltage on the centre conductor.

FIELD-EMISSION TEST ON CEBAF

In January 2017, a 12-m fibre and diamond detectors were tested with field emission from the last cryomodule (1L26, a high-gradient C100) of the CEBAF north linac, in collaboration with Rongli Geng of Jefferson Lab [10]. RF was on for the full linac, without photocurrent. The

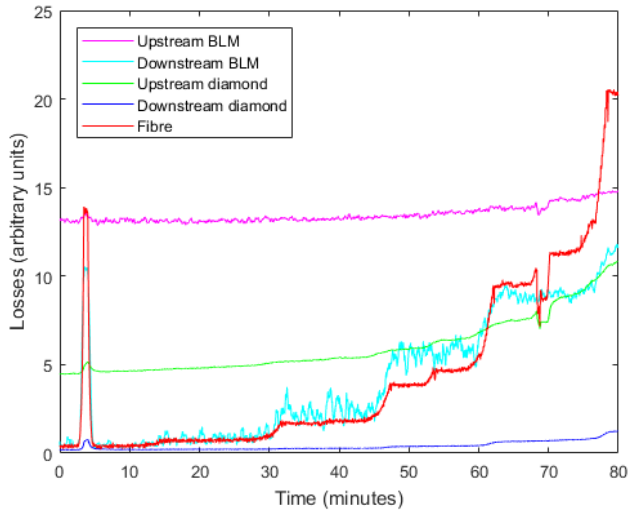

Figure 5: Losses from field-emission at CEBAF.

fibre was draped along the length of the 10-m module; a high-radiation (B4) diamond and a CEBAF scintillating beam-loss monitor (BLM) were at each end. In Fig. 5, as the field gradients in the 8 cavities of 1L26 were stepped sequentially by 1 MeV/m, the upstream BLM and diamond were dominated by losses from the previous module (1L25), but the fibre responded only to 1L26 and was sensitive to losses from the interior cavities. It showed strong growth in field emission from cavity 7 at the highest gradients and highlighted an upward spike from cavity 7 at $t = 4$ and a drop-out of cavity 3 at $t = 68$.

REFERENCES

[1] P. Emma *et al.*, "First lasing and operation of an ångstrom-wavelength free-electron laser", Nature Photonics **4** (2010) 641.

[2] LCLS-II Final Design Report, LCLSII-1.1-DR-0251-R0, 2105-11-22.

[3] FACET-II Conceptual Design, 2015-09-02.

[4] Alan S. Fisher, Clive Field, Ludovic Nicolas, "Evaluating Beam-Loss Detectors for LCLS-2", in *Proc. Int. Beam Instrumentation Conf.*, Barcelona, Spain, Sept. 2016, 678.

[5] K. Cankoçak *et al.*, "Radiation-hardness measurements of high OH^- content quartz fibres irradiated with 24-GeV protons up to 1.25 Grad", Nucl. Instrum. Methods A **585** (2008) 20.

[6] I. Dumanoglu *et al.*, "Radiation-hardness studies of high OH^- content quartz fibres irradiated with 500-MeV electrons", Nucl. Instrum. Methods A **490** (2002) 444.

[7] M. Santana Leitner, "Fluence to dose conversion E-curves for silicon and polyethylene. A FLUKA user-routine to convert fluence into energy deposition in small radiation sensitive accelerator components", SLAC Radiation Physics Note RP-14-20, example 3, dose near a stopper.

[8] Hamamatsu measurement of an H11901P-01 PMT module.

[9] CIVIDEC, https://cividec.at/

[10] R.L. Geng, A. Freyberger, R. Legg, R. Suleiman, A.S. Fisher, "Field Emission in SRF Accelerators: Instrumented Measurements for its Understanding and Mitigation," presented at IBIC'17, Grand Rapids, MI, USA, Aug. 2017, paper TH1AB1.